

KMC Simulation of the Electroforming, Set and Reset Processes in Redox-based Resistive Switching Devices

Elhameh Abbaspour
 Institute of Electromagnetic Theory
 RWTH Aachen University
 Aachen 52056, Germany
 Email: ea@ithe.rwth-aachen.de

Stephan Menzel
 Peter Grünberg Institut
 Forschungszentrum Jülich
 52425 Jülich, Germany
 Email: st.menzel@fz-juelich.de

Christoph Jungemann
 Institute of Electromagnetic Theory
 RWTH Aachen University
 Aachen 52056, Germany
 Email: cj@ithe.rwth-aachen.de

Abstract—This paper presents a physical model based on charge transport in order to investigate the electroforming and switching processes of ReRAMs. This model is based on the generation and annihilation of oxygen vacancies (V_{O}) along the metal-oxide interfaces and their migration through the oxide. The major driving forces governing these processes are the electric field, temperature and temperature gradient. Our simulations reproduce the main switching characteristics like the abrupt set and gradual reset processes. The variability of the switching parameters is also studied here as one of the major challenges of ReRAM mass production.

I. INTRODUCTION

Redox-based resistive switching RAM (ReRAM) is currently considered as a promising candidate for future nonvolatile memory application due to its high scalability potential and compatibility with CMOS technology and simple structure [1]. Typically an initial one-time operation, named electroforming process, which is regarded as a soft dielectric breakdown, is required to generate the metal-rich conducting filaments (CF) inside the oxide [1]. When a CF, which may consist of V_{O} [2], [3], is generated, it connects the top and bottom electrodes and the ReRAM switches to low resistance state (LRS). The filament rupture brings the device back to high resistance state (HRS).

Despite the major progress in understanding the forming process, a comprehensive study of the microscopic properties of the CF, which is determined during the forming process and has a great effect on the switching properties, is still missing [4], [5]. Understanding these features allows us to avoid arbitrary assumptions about forming characteristics and study directly the role of forming conditions on the switching process.

In this study a kinetic Monte Carlo (KMC) code has been developed to simulate the whole switching process in a HfO_2 -based ReRAM continuing our previously presented forming model [6]. Studies show that the generation and annihilation of the Frenkel defect pairs inside bulk is either energetically unfavorable or unstable [7]–[9]. Therefore in this model V_{O} s can only be introduced into the system by oxygen exchange along metal-oxide boundaries. In contrast, most of the previous works used bulk models where V_{O} and oxygen interstitials could also be created

and recombined inside the bulk [5], [10]–[12]. With our interface model similar forming and switching features are captured as with the previous models [10], [12], [13]. Despite the fact that the poor uniformity of the switching parameters is one of the most well-known issues regarding ReRAM, the origin of these fluctuations is not well understood yet [12]. In order to have a better understanding of this issue variations of the resistances in HRS and LRS has been studied in this work.

II. MODEL DESCRIPTION

The building blocks in Fig. 1 illustrate the simulation flow of the forming and switching processes in this work. It starts with the modeling of the forming process and an initial distribution of V_{O} s along grain boundaries (GB) [10]. The V_{O} distribution at each time determines the charge transport mechanism. At low V_{O} concentration we have direct tunneling (DT) and defect-defect tunneling (DDT) conduction mechanisms. Here DT means the injection of electrons from the electrode into a V_{O} and vice versa. In this case the tunneling probabilities are given by the Wentzel–Kramers–Brillouin (WKB) approximation,

$$TP(E) = e^{-2 \int_{x_0}^{x_1} dx \frac{1}{\hbar} \sqrt{2m^*(V-E)}} \quad (1)$$

where TP is the tunneling probability between electrodes and traps, x_0 and x_1 are two edges of the tunneling process, $m^* = 0.1m_0$ is the HfO_2 tunneling effective mass and E and V are particle energy and tunneling barrier respectively.

V_{O} s play the role of traps where electrons can jump through them and control the leakage current through the oxide. The hopping rate of electrons between traps is calculated using the Miller-Abrahams formula,

$$h_{nm} = \begin{cases} \nu_{0n} \exp \left[-\frac{d_{nm}}{a_0} + \frac{q(V_n^H - V_m^H)}{k_B T} \right] & V_n^H \leq V_m^H \\ \nu_{0n} \exp \left[-\frac{d_{nm}}{a_0} \right] & V_n^H > V_m^H \end{cases} \quad (2)$$

with h_{nm} and d_{nm} being the hopping rate of electrons and the distance between trap n and m , respectively, V_n^H and V_m^H being the homogenous potential of traps n and m , ν_{0e} being the electron characteristic vibration frequency and k_B being the Boltzmann constant.

We have developed a trap assisted tunneling (TAT) current solver including DT and DDT mechanisms for low V_{O}

concentration to calculate the electron flux through one of the electrodes,

$$I_{TAT} = e \sum_{n=1}^N [p_n H_{na} - (1 - p_n) H_{an}] \quad (3)$$

where e is the electron charge, N is the total number of traps, p_n is the occupational probability of trap n and H_{na} and H_{an} are the rates of an electron hop from trap n to the anode and vice versa. The current continuity equation for the quasi-steady state is solved self-consistently with Poisson equation in order to calculate the occupational probabilities of the traps,

$$(1 - p_n) \sum_{m=1, m \neq n}^N p_m h_{mn} - p_n \sum_{m=1, m \neq n}^N (1 - p_m) h_{nm} \quad (4)$$

$$+ (H_{cn} + H_{an})(1 - p_n) - (H_{nc} + H_{na})p_n = 0.$$

At high $V_{\bar{o}}$ concentration direct drift occurs and we solve drift-diffusion equations self-consistently with the Poisson equation in order to calculate the device current. The Fourier heat-flow equation is solved to determine the temperature profile T ,

$$\nabla \cdot (k_{th} \nabla T) = -P, \quad (5)$$

where k_{th} is the oxide thermal conductivity and P is the power dissipation inside the oxide, which can be easily calculated with voltage and current.

Then, using the KMC method it is determined which of the following processes with corresponding transition rates would happen at the next step,

- $V_{\bar{o}}$ generation, $G_i = \nu_0 \exp\left(-\frac{E_G - \alpha q F_{ext}}{k_B T}\right)$
- $V_{\bar{o}}$ annihilation, $R_i = \nu_0 \exp\left(-\frac{E_R + \alpha q F_{ext}}{k_B T}\right)$
- $V_{\bar{o}}$ diffusion, $D_{i,j} = \nu_0 \exp\left(-\frac{E_D - \alpha q \nabla V_{ij} - k_B a \nabla T}{k_B T}\right)$

where, ν_0 is the characteristic vibration frequency, E_G , E_R and E_D are the activation energies of $V_{\bar{o}}$ generation, annihilation and diffusion, α is the symmetry factor, a the lattice constant, F_{ext} the locally induced electric field and ∇V_{ij} the diffusion barrier change due to the site potential. As soon as the device current is greater than a predefined compliance current, the forming process stops and the switching process continues for a given number of loops, with new set and reset voltages. The simulation flow for the switching process is the same as for the forming.

Table I contains the main parameters used in our simulation.

TABLE I. THE MAIN MODEL PARAMETERS

ν_0	ν_{0e}	E_G	E_R	E_D	α	k_{th}
10^{13} Hz	10^{12} Hz	3.0e V	1.0e V	0.7e V	0.5	0.5 (W/Km)

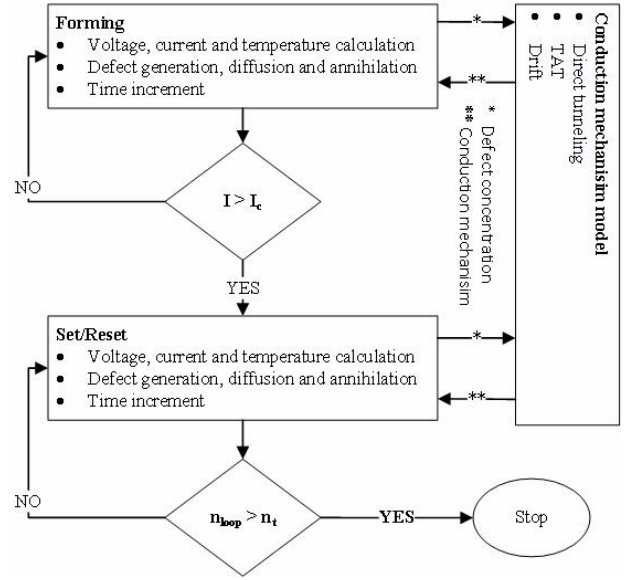


Fig. 1. Flowchart of the KMC simulation flow to study the forming and switching processes, where n_{loop} and n_t are the current loop and the total number of switching loops, respectively.

III. SIMULATION RESULTS AND DISCUSSION

A. Forming Process

The formation of a CF under an applied ramp voltage has been simulated using our KMC forming model. Fig. 2(a) and 2(b) shows the $I - V$ characteristics and $V_{\bar{o}}$ and temperature distribution during the forming process, respectively. The forming simulation starts with an initial random distribution of $V_{\bar{o}}$ along GB and stops when the current compliance, I_c is reached. The results show that generation of $V_{\bar{o}}$ mostly happens at high voltage and temperature.

The role of the external temperature in the forming process has been studied as shown in Fig. 3(a) and 3(b). The results indicate a reduction in forming voltage by increasing temperature. This is due to the strong dependence of the $V_{\bar{o}}$ generation process on the temperature. For higher temperature the Hf-O bond breakage happens at lower voltages, therefore the forming voltage decreases.

In order to investigate the effect of the current compliance on CF properties the forming step has been simulated for 3 different current levels $I_c = 100 \mu A$, $I_c = 500 \mu A$ and $I_c = 1000 \mu A$. Figure. 4(a), 4(b) and 4(c) show the results. For smaller I_c the CF is thinner and has a smaller $V_{\bar{o}}$ density and this leads to more CF instability.

B. Set and Reset Process

After the forming step is completed, the simulation continues with the set/reset processes. The $I - V$ characteristics for 3 switching loops and the corresponding $V_{\bar{o}}$ and temperature distribution at the end of the set and reset processes are shown in Fig. 5(a) and 5(b), respectively. The $I - V$ figure shows an expected abrupt set process and a gradual reset process. Annihilation of a part of the

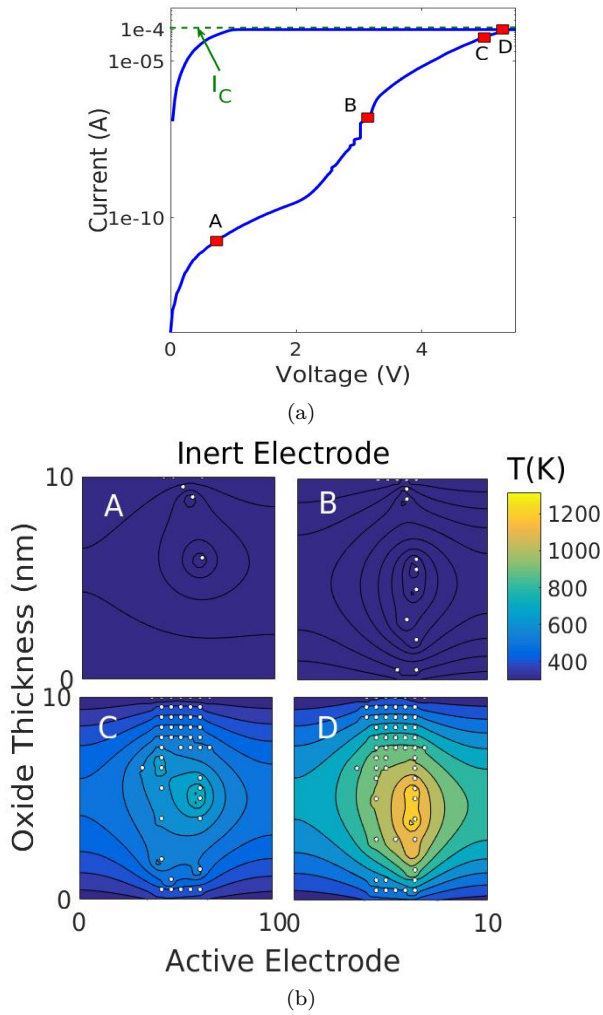


Fig. 2. (a) Simulated $I - V$ characteristics in a forming process in a TiN/10 nm HfO₂/Pt cell at $I_C = 100 \mu A$ (b) The evolution of the V_δ distribution and temperature along CF during the forming process in the same cell at different stages A ($V = 0.5$ V), B ($V = 3.0$ V), C ($V = 5.0$ V), D ($V = V_f = 5.3$ V)

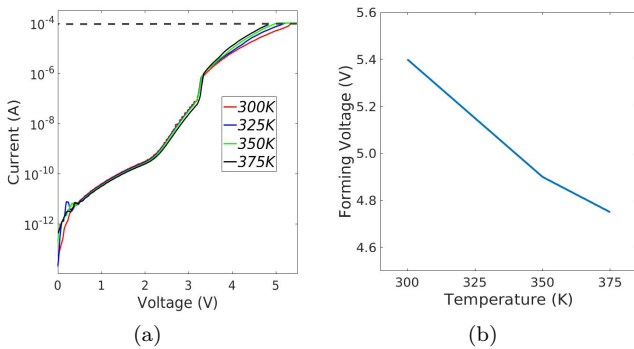


Fig. 3. (a) $I - V$ curve in a TiN/10 nm HfO₂/Pt cell at different temperatures (b) Forming voltage as a function of the external temperature

CF during the reset and reconstruction of this part in set can be observed in the distribution figures.

The distributions of the forming, set and reset voltages in Fig. 6(a) show the highest fluctuation for the reset volt-

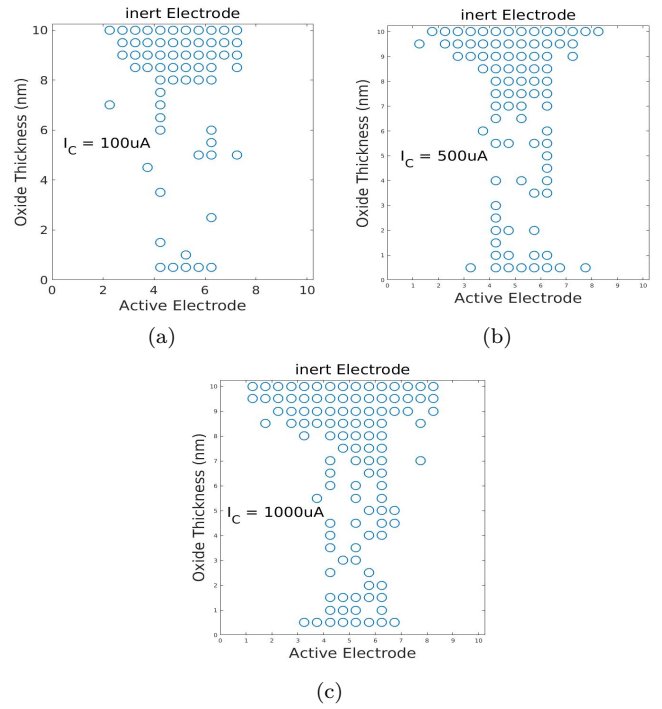


Fig. 4. CF generation at the end of the forming process for different current compliances (a) $I_C = 100 \mu A$ (b) $I_C = 500 \mu A$ (c) $I_C = 1000 \mu A$

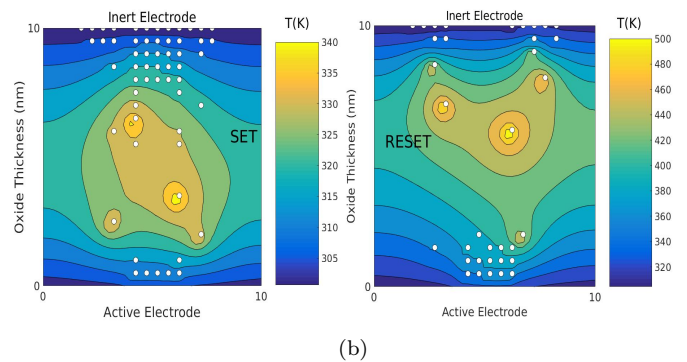
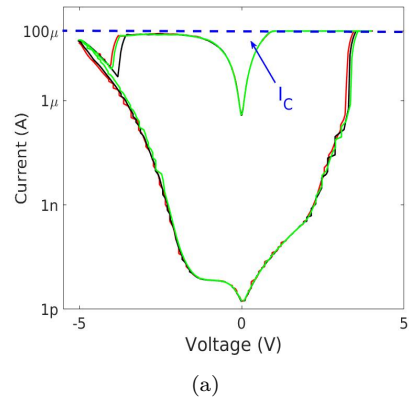


Fig. 5. (a) $I - V$ characteristics of set and reset processes for 3 switching loops (b) V_δ and temperature distributions at the end of set ($V_{set} = 4$ V) and reset ($V_{reset} = -5$ V) processes

age. This is consistent with the results of the distribution of LRS and HRS resistances, in Fig. 6(b) which show a

REFERENCES

- [1] R. Waser, R. Dittmann, G. Staikov, and K. Szot, "Redox-Based Resistive Switching Memories – Nanoionic Mechanisms, Prospects, and Challenges," *Advanced Materials*, vol. 21, no. 25-26, pp. 2632–2663, 2009.
- [2] K. M. Kim, B. J. Choi, Y. C. Shin, S. Choi, and C. S. Hwang, "Anode-interface localized filamentary mechanism in resistive switching of TiO₂ thin films," *Applied Physics Letters*, vol. 91, no. 1, 2007.
- [3] E. Miranda, C. Walczyk, C. Wenger, and T. Schroeder, "Model for the Resistive Switching Effect in HfO₂ MIM Structures Based on the Transmission Properties of Narrow Constrictions," *Electron Device Letters, IEEE*, vol. 31, no. 6, pp. 609–611, 2010.
- [4] P. Gonon, M. Mougnot, C. Vallée, C. Jorel, V. Jousseau, H. Grampeix, and F. El Kamel, "Resistance switching in HfO₂ metal-insulator-metal devices," *Journal of Applied Physics*, vol. 107, no. 7, 2010.
- [5] B. Butcher, G. Bersuker, D. Gilmer, L. Larcher, A. Padovani, L. Vandelli, R. Geer, and P. Kirsch, "Connecting the physical and electrical properties of Hafnia-based RRAM," *Electron Devices Meeting (IEDM), 2013 IEEE International*, pp. 22.2.1–22.2.4, 2013.
- [6] E. Abbaspour, C. Jungemann, and S. Menzel, "The role of the interface reactions in the electroforming of redox-based resistive switching devices using KMC simulations," pp. 293 – 296, 2015.
- [7] A. O'Hara, G. Bersuker, and A. A. Demkov, "Assessing hafnium on hafnia as an oxygen getter," *Journal of Applied Physics*, vol. 115, no. 18, 2014.
- [8] S. Clima, B. Govoreanu, M. Jurczak, and G. Pourtois, "HfO_x as RRAM material – First principles insights on the working principles," *Microelectronic Engineering*, vol. 120, pp. 13 – 18, 2014.
- [9] Y. Guo and J. Robertson, "Materials selection for oxide-based resistive random access memories," *Applied Physics Letters*, vol. 105, no. 22, 2014.
- [10] G. Bersuker, D. C. Gilmer, D. Veksler, P. Kirsch, L. Vandelli, A. Padovani, L. Larcher, K. McKenna, A. Shluger, V. Iglecias, M. Porti, and M. Nafria, "Metal oxide resistive memory switching mechanism based on conductive filament properties," *Journal of Applied Physics*, vol. 110, no. 12, 2011.
- [11] A. Padovani, L. Larcher, O. Pirrotta, L. Vandelli, and G. Bersuker, "Microscopic modeling of hfox rram operations: From forming to switching," *IEEE Transactions on Electron Devices*, vol. 62, no. 6, pp. 1998–2006, 2015.
- [12] X. Guan, S. Yu, and H.-S. Wong, "On the Switching Parameter Variation of Metal-Oxide RRAM; Part I: Physical Modeling and Simulation Methodology," *Electron Devices, IEEE Transactions on*, vol. 59, no. 4, pp. 1172–1182, 2012.
- [13] F. M. Puglisi, D. Deleruyelle, J.-M. Portal, P. Pavan, and L. Larcher, "A multi-scale methodology connecting device physics to compact models and circuit applications for oxram technology," *physica status solidi (a)*, vol. 213, no. 2, pp. 289–301, 2016.

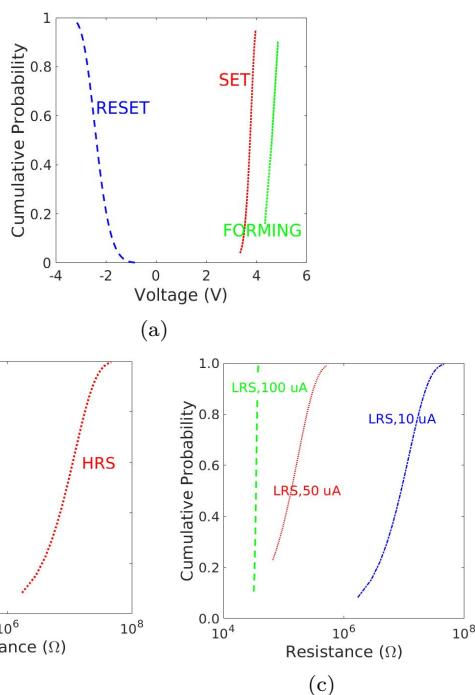


Fig. 6. Simulation results of the Weibull distribution of (a) the forming, set and reset voltages for $I_c = 50 \mu\text{A}$, (b) the LRS and HRS resistance for $I_c = 100 \mu\text{A}$ (c) the LRS resistance for different current compliance

higher variation of HRS resistance than LRS resistance. The effect of current compliance on the variability of the LRS resistance is shown in Fig. 6(c). As we saw in Fig. 4, the higher current compliance resulted in more CF stability and we can see the same result here. For higher I_c the LRS resistance has less variation.

IV. CONCLUSION

We presented a KMC approach in this paper to simulate the complete resistive switching process in a HfO₂-based ReRAM, in which oxygen vacancies can only be introduced at the ohmic interface and not within the bulk. Our model used a combination of conduction mechanisms to catch the key features of the forming and switching processes and studied the effect of forming conditions on forming and switching characteristics. We also investigated the fluctuation of the switching parameters as one of the major issue of ReRAM large-scale production.

ACKNOWLEDGMENT

This work was supported by the Deutsche Forschungsgemeinschaft under Grant SFB 917.